1418 *Biochemistry* **2010,** *49,* 1418–1424
DOI: 10.1021/bi901617w

BIOCHEMISTRY
including biophysical chemistry & molecular biology
*Article*

# Mechanism of Binding of the Inhibitor (*E*)-3-(Furan-2-yl)-*N*-hydroxyacrylamide to a Histone Deacetylase-like Amidohydrolase

Jaromir Sykora and Franz-Josef Meyer-Almes*

*Department of Chemical Engineering and Biotechnology, University of Applied Sciences, Schnittspahnstrasse 12, 64287 Darmstadt, Germany*

*Received September 16, 2009; Revised Manuscript Received December 23, 2009*

ABSTRACT: Histone deacetylases have proven to be attractive novel targets for the treatment of cancer. The first inhibitor of histone deacetylases was approved for the treatment of cutaneous T-cell lymphoma in 2006. The identification of new lead structures with improved effectiveness and fewer side effects is necessary. This report investigates the mechanism of inhibition of a histone deacetylase-like amidohydrolase by stopped-flow and equilibrium titration techniques. The interaction between the inhibitor (*E*)-3-(furan-2-yl)-*N*-hydroxyacrylamide and the enzyme generates a fluorescence resonance energy transfer from the intrinsic tryptophan residues of the enzyme to the chromophore of the inhibitor. The apparent equilibrium binding constant was determined to be 1.9 $\mu$M. Several independent experimental results provide evidence of the existence of solely one HDAH conformer. The association kinetics showed two phases representing two unimolecular processes. Kinetic arguments and accurate investigation of the very fast time range suggest a fast pre-equilibrium, in which the inhibitor binds to the surface of the enzyme. In the next step, the first complex undergoes a conformational change that allows the inhibitor to translocate into the active site. Finally, the intermediate complex is stabilized by another conformational rearrangement. All kinetic data are in agreement with a reversible three-step mechanism and analyzed using a global fit, yielding the association constant of the pre-equilibrium ($K_1 = 0.28 \times 10^6$ $M^{-1}$) and the forward and reverse rate constants of the consecutive conformational changes ($k_2 = 6.6$ $s^{-1}$, $k_{-2} = 1.5$ $s^{-1}$, $k_3 = 0.8$ $s^{-1}$, and $k_{-3} = 0.3$ $s^{-1}$).

The regulation of the acetylation status of histones plays an important role in transcription regulation of eukaryotic cells (*1*, *2*). Histones are acetylated by histone acetyltransferases (HATs)[1] and deacetylated by histone deacetylases (HDACs). Increased levels of histone acetylation promote relaxation of chromatin structure. In humans, 18 HDAC enzymes have been identified and divided into four classes. Class I, II, and IV enzymes depend on $Zn^{2+}$, whereas the members of class III, the so-called sirtuins, require $NAD^+$ for their enzymatic activity. In general, HDACs can act as transcription repressors due to histone deacetylation and promotion of chromatin condensation (*3*, *4*). Despite this fundamental mode of action, which appears to be rather unselective, HDAC inhibitors seem to directly affect transcription of only a relatively small number of genes (*5*, *6*). Most of these genes are involved in the control of cell growth and survival, providing a rationale for the anticancer activity of HDAC inhibitors. In addition, there are many non-histone protein substrates, e.g., hormone receptors, chaperone proteins, and cytoskeleton proteins, which regulate cell proliferation and cell death (*7*). Therefore, HDAC inhibitors act through transcription-dependent and transcription-independent mechanisms (*8*, *9*). Several classes of synthetic compounds and natural products have been reported to inhibit HDACs (reviewed in ref *10*). Furthermore, a small number of drug candidates are currently in phase I−III clinical trials, as reviewed by Riester et al. (*11*) and Lee et al. (*12*). Recently, the first HDAC inhibiting drug, vorinostat (Zolinza, Merck & Co.; SAHA), has been approved by the U.S. Food and Drug Administration (FDA) for the treatment of cutaneous T-cell lymphoma as the first compound in class. The development of further HDAC inhibitors offers new opportunities in the treatment of cancer. The histone deacetylase-like amidohydrolase (HDAH) from *Bordetella* serves as a validated model for HDAC6 with regard to both structure (*13*) and function (*14*). The level of sequence identity of HDAH with the second domain of HDAC6 is 35%. Both enzymes share similar substrate and inhibitor selectivities (*15*, *16*). It has been shown that SAHA and other hydroxamates bind to HDAH via their hydroxamate group which interacts with the $Zn^{2+}$ ion inside the active site of HDAH (*13*, *17*). (*E*)-3-(Furan-2-yl)-*N*-hydroxyacrylamide (FAHA), another hydroxamate, binds to HDAH and inhibits eukaryotic HDACs (*18*). The interaction of FAHA with HDAH can be measured instantaneously by exploiting the fluorescence resonance energy transfer (FRET) from the intrinsic tryptophans of HDAH to FAHA which has been shown to occur upon binding (*18*).

This study aimed to produce a more detailed mechanistic view of histone deacetylase inhibition and to complement the static picture of previously determined crystal structures of HDAH−inhibitor and HDAC−inhibitor complexes.

## EXPERIMENTAL PROCEDURES

*Reagents*. (*E*)-3-(Furan-2-yl)-*N*-hydroxyacrylamide (FAHA) and suberoylhydroxamic acid (SAHA) were synthesized according

*To whom correspondence should be addressed: University of Applied Sciences, Schnittspahnstr. 12, 64287 Darmstadt, Germany. Telephone: ++49-6151168406. Fax: ++49-6151168404. E-mail: franz-josef.meyer-almes@h-da.de.

[1]Abbreviations: CypX, cyclopentylpropionyl hydroxamate; FAHA, (*E*)-3-(furan-2-yl)-*N*-hydroxyacrylamide; EDTA, ethylenediaminetetraacetic acid; FRET, fluorescence resonance energy transfer; HAT, histone acetyltransferase; HDAC, histone deacetylase; HDAH, histone deacetylase-like amidohydrolase from *Bordetella*/*Alcaligenes* FB188; SAHA, suberoylanilide hydroxamic acid; TRIS, tris(hydroxymethyl)-aminomethane.

 Published on Web 01/18/2010 

to the standard methods (*13*, *18*−*20*). His-tagged HDAH from *Bordetella*/*Alcaligenes* was prepared as described previously (*14*). All other reagents were obtained from Sigma (Taufkirchen, Germany). All binding and displacement reactions were conducted under standard assay conditions in 250 mM NaCl, 250 μM EDTA, 15 mM Tris-HCl, and 50 mM potassium phosphate (pH 8.0) at 21 °C.

*Equilibrium Binding*. HDAH (250 nM) was titrated with increasing concentrations of FAHA. We assessed the formation of the FAHA−HDAH complex by exploiting the fluorescence resonance transfer from the donor tryptophans of HDAH to the acceptor furylacryloyl chromophore of FAHA. The intrinsic HDAH tryptophans were excited at 285 nm (slit width 5 nm), and their fluorescence emission was measured at 350 nm (slit width 10 nm) in a Hitachi F-7000 spectrofluorometer. The binding data were fitted to the so-called four-parameter logistic function using Origin (OriginLab Corp.):

$$\mathrm{RFU} = P_2 + \frac{P_1 - P_2}{1 + \left[\frac{c(\mathrm{FAHA})}{P_3}\right]^{P_4}} \quad (1)$$

where $P_1$ denotes the low and $P_2$ the high plateau, $P_3$ is the $IC_{50}$ value, and $P_4$ is a measure for the steepness of the curve. Since the concentration of FAHA was ~10 times higher than the concentration of HDAH at the point of inflection, the $IC_{50}$ value is equivalent to the binding constant $K_D$ within the experimental variance.

*Stopped-Flow Kinetics*. The measurements of binding and displacement kinetics were conducted on a Bio-Logic MOS-250 stopped-flow instrument which was described in detail previously (*18*). The intrinsic tryptophans of HDAH were excited at 285 nm by a 150 W xenon mercury light source, which was attached to a manual monochromator, and the emitted fluorescence light was measured after it had passed through a polystyrene cutoff filter to reject scattered light. The data were fitted to either a monophasic or biphasic exponential model by using a nonlinear least-squares fitting procedure integrated in BioKine32. The dead time of the instrument was calculated to be < 2 ms. The temperature was controlled at 21 ± 0.2 °C.

*Reaction Mechanism*. (*i*) *One-Step Reaction*. In a simple one-step equilibrium, mixing of the reaction partners generates a pure one-exponential binding curve under pseudo-first-order conditions. The reciprocal time constant ($1/\tau$) depends linearly on the concentration of reaction partner B being in high excess over the other one:

$$\mathrm{A} + \mathrm{B} \underset{k_{-1}}{\overset{k_1}{\rightleftharpoons}} \mathrm{C}$$

$$\frac{1}{\tau} = k_1 B_0 + k_{-1} \quad (2)$$

where $k_1$ and $k_{-1}$ denote the association and dissociation rate constants, respectively. Deviations from linearity indicate a more complex reaction mechanism.

(*ii*) *Two-Step Reaction*. In many cases, the initial bimolecular recognition step is followed by an unimolecular step, e.g., a conformational rearrangement of the first complex. In the case of a fast pre-equilibrium, where $k_1B_0 + k_{-1} \gg k_2, k_{-2}$, and under pseudo-first-order conditions, a biexponential binding curve is obtained, which reflects both consecutive reaction steps. The reciprocal time constant ($1/\tau_1$) of the fast first binding step depends linearly on the concentration of excess reaction partner B like in the one-step reaction mechanism (see eq 2). In contrast, the second reciprocal time constant ($1/\tau_2$) reaches a plateau at higher concentrations of partner B according to the following equation (*21*):

$$\mathrm{A} + \mathrm{B} \underset{k_{-1}}{\overset{k_1}{\rightleftharpoons}} \mathrm{C} \underset{k_{-2}}{\overset{k_2}{\rightleftharpoons}} \mathrm{D}$$

$$\frac{1}{\tau_2} = \frac{k_1 k_2 B_0}{k_1 B_0 + k_{-1}} + k_{-2} \quad (3)$$

where $k_1$ and $k_2$ are the forward rate constants and $k_{-1}$ and $k_{-2}$ are the reverse rate constants of the two-step mechanism. $B_0$ is the molecular species in excess.

(*iii*) *Three-Step Reaction*. A three-step mechanism results, if there are two consecutive steps which, e.g., represent distinct conformational changes after the formation of the initial complex, C. Again, pseudo-first-order conditions with species B in excess simplify the analysis of kinetic data. The three-step reaction is characterized by three relaxation processes. If the pre-equilibrium is established much faster than the subsequent unimolecular steps, e.g., $k_1B_0$, $k_{-1} \gg k_2$, $k_{-2}$, $k_3$, $k_{-3}$, the reciprocal time of the fast pre-equilibrium is the same as for the two-step mechanism and is described by eq 2. By taking the sum and the product of the reciprocal time constants ($1/\tau_2$ and $1/\tau_3$) of the two slower processes, one obtains expressions that allow for the determination of the various rate coefficients (*21*):

$$\mathrm{A} + \mathrm{B} \underset{k_{-1}}{\overset{k_1}{\rightleftharpoons}} \mathrm{C} \underset{k_{-2}}{\overset{k_2}{\rightleftharpoons}} \mathrm{D} \underset{k_{-3}}{\overset{k_3}{\rightleftharpoons}} \mathrm{E}$$

$$\frac{1}{\tau_2} + \frac{1}{\tau_3} = \frac{k_2 K_1 B_0}{1 + K_1 B_0} + k_{-2} + k_3 + k_{-3} \quad (4)$$

$$\frac{1}{\tau_2}\frac{1}{\tau_3} = \frac{k_2 K_1 B_0}{1 + K_1 B_0}(k_3 + k_{-3}) + k_{-2} k_{-3} \quad (5)$$

All time constants measured for several concentrations of $B_0$ (FAHA) are analyzed by a global fit to eqs 4 and 5 to yield the association constant of the pre-equilibrium, $K_1$, and the other rate constants using the generalized reduced gradient algorithm from Lasdon et al. (*22*) implemented in the Solver extension of Microsoft Excel.

*Equations for the Calculation of FRET Efficiencies*. The transfer efficiency ($E$) of a FRET system can be calculated according to the well-known expression given by Foerster (*23*):

$$E = \frac{{R_0}^6}{{R_0}^6 + R^6} \quad (6)$$

where $R_0$ is the so-called Foerster distance and $R$ is the distance between donor and acceptor. $E$ becomes 0.5, if $R$ equals $R_0$. Rearrangement of eq 6 for two different distances ($R_i$ and $R_s$) and elimination of $R_0$ give

$$E_s = \frac{{R_i}^6 E_i}{(1 - E_i){R_s}^6 + E_i {R_i}^6} \quad (7)$$

where $E_i$ and $E_s$ denote the FRET efficiencies corresponding to distances $R_i$ and $R_s$, respectively. If $E_i$ at a given distance $R_i$ is known, $E_s$ at distance $R_s$ can be calculated for the same donor−acceptor system.

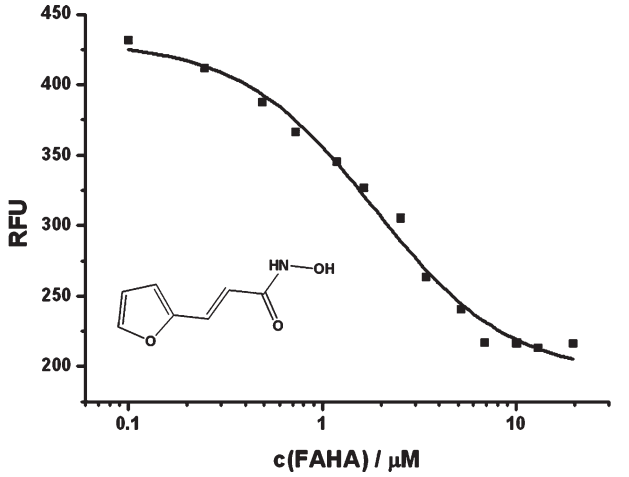


FIGURE 1: Equilibrium binding of FAHA to HDAH. The fluorescence intensity of 250 nM HDAH [$\lambda_{exc}$ = 285 nm (5 nm), and $\lambda_{em}$ = 350 nm (10 nm)] is plotted vs the concentration of FAHA. The assay was performed under standard assay conditions. The data were fitted using eq 1. The binding constant was calculated to be 1.9 $\mu$M. The chemical structure of FAHA is shown under the curve.

## RESULTS

*Equilibrium Titration*. Originally, FAHA was developed as a chemical probe to assay inhibitors of HDAH and HDAC (*18*). FAHA binds to the enzyme in a reversible manner with a binding constant of 1.9 $\mu$M and generates a fluorescence resonance energy transfer (FRET) from the intrinsic tryptophans of the enzyme to FAHA, thereby reducing the donor fluorescence intensity (Figure 1).

In this assay, compounds that bind to the active site of HDAH displace FAHA and recover the tryptophan fluorescence of unbound HDAH again. The energy transfer efficiency ($E$) of the FRET was calculated from the quenching of HDAH donor fluorescence to be 0.53.

*Binding Kinetics*. The FRET signal, which occurs instantaneously upon binding of FAHA to HDAH, allows for a detailed analysis of the kinetics and the mechanism of the interaction. FAHA is a hydroxamate and belongs to the same structural class of HDAC inhibitors as the approved drug SAHA. Therefore, FAHA is a good model for the binding of hydroxamate inhibitors.

FAHA and HDAH were mixed in a stopped-flow instrument to resolve fast binding steps. The concentration of HDAH was 250 nM throughout all experiments, and the concentration of FAHA was varied and at least 8 times higher than the enzyme concentration enabling pseudo-first-order kinetics. The binding of FAHA to HDAH shows a biphasic decrease in tryptophan fluorescence (Figure 2). Alternating mixing experiments of HDAH with buffer and 10 $\mu$M FAHA revealed that there was no detectable very fast unresolved change in the fluorescence signal during the dead time of the instrument.

*Dissociation Kinetics*. To measure the dissociation kinetics of the FAHA−HDAH complex, we formed the complex by mixing 500 nM HDAH and 20 $\mu$M FAHA under standard assay conditions. The solution with the FAHA−HDAH complex was mixed with an equal volume of 500 $\mu$M hydroxamate inhibitor SAHA (Figure 3). The high excess concentration of SAHA over FAHA prevented rebinding and distortion of the displacement kinetics. The apparent dissociation constant was determined from a fit of the kinetic data to a monoexponential function to be 0.15 $s^{-1}$.

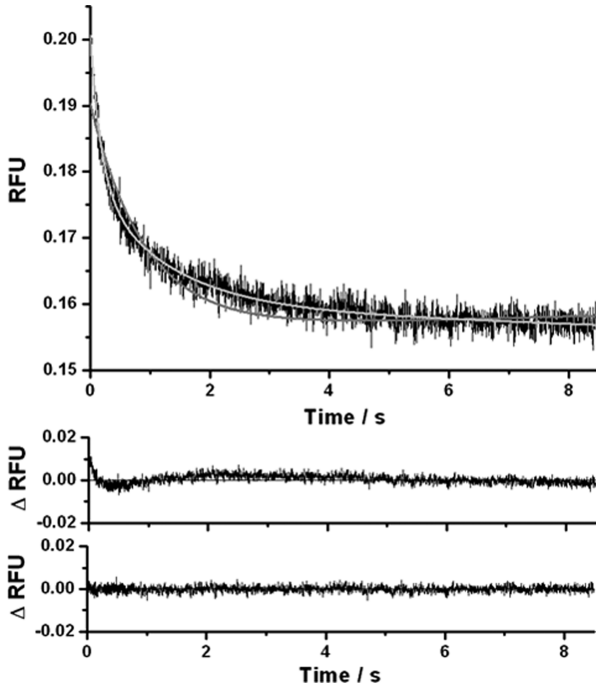


FIGURE 2: Association kinetics of FAHA and HDAH. HDAH (250 nM) and FAHA (10 $\mu$M) were mixed in standard assay buffer at pH 8.0 and 21 °C. The fluorescence intensity of HDAH is plotted vs time after complete mixing. The data were fit to a monophasic (dark gray line) and a biphasic exponential model (light gray line). The biphasic exponential model yielded inverse time constants ($1/\tau$) of 5.47 and 0.79 $s^{-1}$, respectively. The deviations (ΔFluo) between data and the fit to the monophasic (middle) and biphasic exponential model (bottom) vs time are shown below.

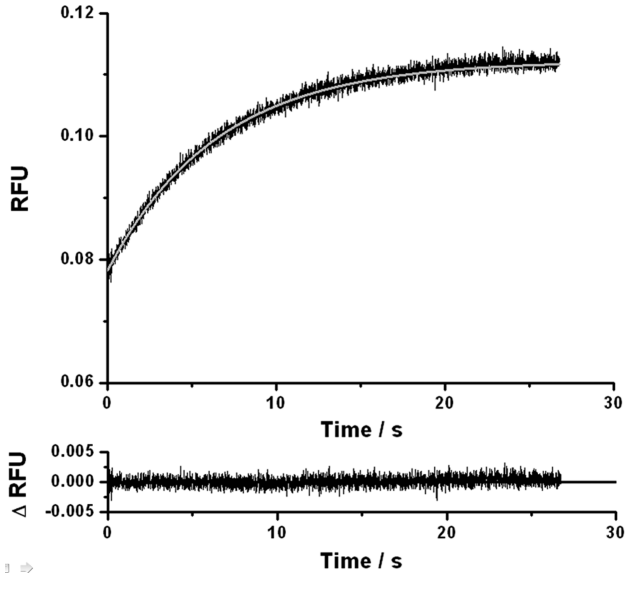


FIGURE 3: Dissociation kinetics of FAHA and HDAH. SAHA (250 $\mu$M) was added to a preformed complex of 250 nM HDAH and 10 $\mu$M FAHA. The fluorescence intensity of HDAH is plotted vs time. The data were fit to a monophasic function, yielding an off rate of 0.15 $s^{-1}$. The deviation between data and the fit curve (gray line) vs time is shown below.

*Reaction Mechanism*. The equilibrium and kinetic data are in agreement with a three-step mechanism consisting of a fast pre-equilibrium and two consecutive conformational changes of the intermediate complexes. Under the assumption of a fast pre-equilibrium, namely, $k_1B_0$, $k_{-1} \gg k_2$, $k_{-2}$, $k_3$, $k_{-3}$, and

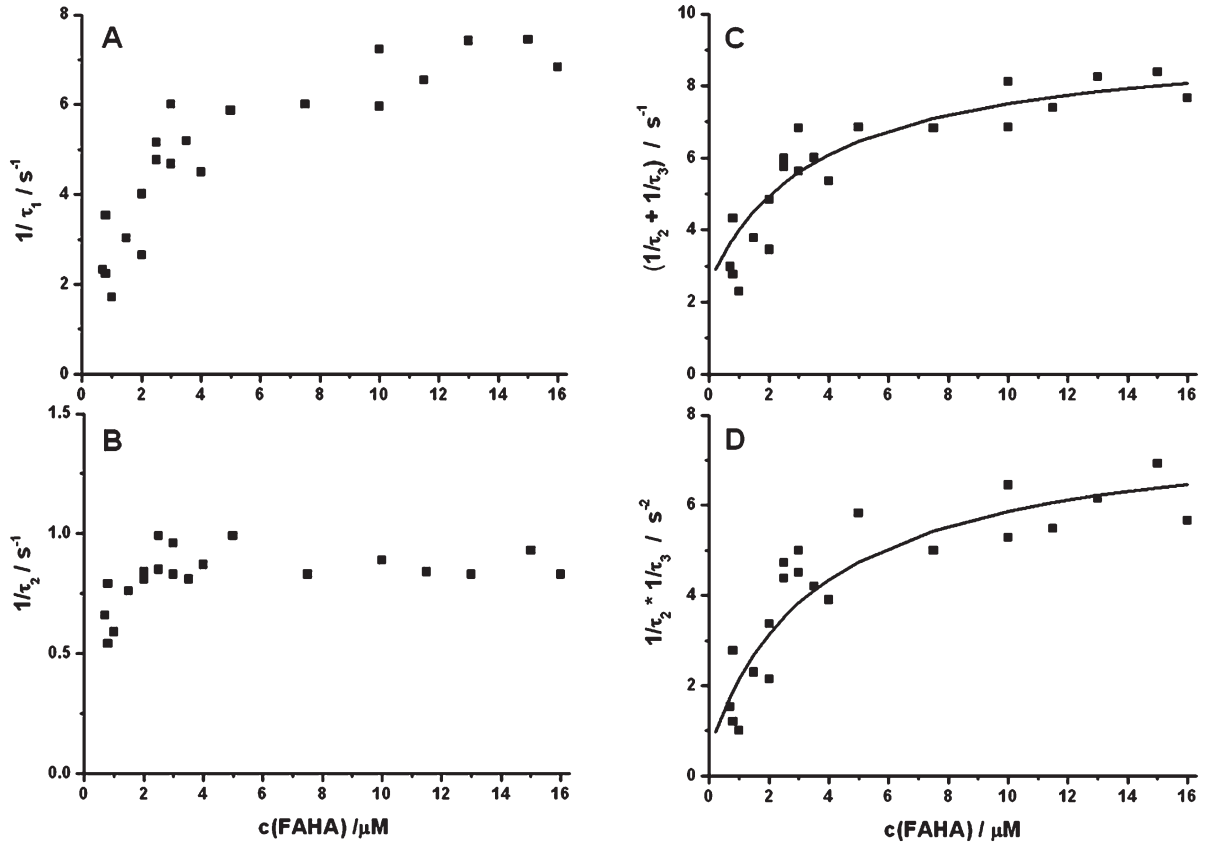


FIGURE 4: Analysis of the biphasic association kinetics. The single reverse reciprocal time constants [$1/\tau_1$ (A) and $1/\tau_2$ (B)] as well as their sum (C) and product (D) obtained from stopped-flow experiments are plotted vs the concentration of excess FAHA that was mixed with 250 nM HDAH in all experiments. The experiments were performed under standard assay conditions. The sets of data in panels C and D were globally fit to a consecutive three-step reaction model according to eqs 4 and 5, yielding the following values: $K_1 = 0.28 \times 10^6\ M^{-1}$, $k_2 = 6.6\ s^{-1}$, $k_{-2} = 1.5\ s^{-1}$, $k_3 = 0.8\ s^{-1}$, and $k_{-3} = 0.3\ s^{-1}$.

pseudo-first-order conditions, the sum and the product of both inverse slow experimental time constants can be analyzed in a straightforward manner. The binding constant of the pre-equilibrium and the various rate constants are obtained from a global fit of both data sets, the sum and product of the two inverse time constants versus FAHA concentration, to eqs 4 and 5 (Figure 4C, D). The association constant of the first binding step ($K_1$) was determined to be $0.28 \times 10^6\ M^{-1}$, and the rate constants of the subsequent steps are as follows: $k_2 = 6.6\ s^{-1}$, $k_{-2} = 1.5\ s^{-1}$, $k_3 = 0.8\ s^{-1}$, and $k_{-3} = 0.3\ s^{-1}$.

## DISCUSSION

The bacterial HDAC homologue HDAH and FAHA have been chosen as a model system for investigating the mechanism of inhibition of HDACs, which have become key targets for drug treatment in recent years. FAHA proved to be a well-suited tool for the creation of an efficient FRET from the tryptophans of HDAH to the chromophoric system of FAHA, leading to a strong quench of the fluorescence emission of the tryptophan residues upon binding (Figure 1). This enables detailed studies of the interaction of HDAH and the model inhibitor FAHA in a homogeneous solution. The generated FRET signal not only indicates the very fast progress of the binding reaction but also contains information about the distance between the donor tryptophans of HDAH and the chromophoric system of FAHA.

A titration of 250 nM HDAH with increasing concentrations of FAHA under standard assay conditions revealed an apparent binding constant of 1.9 $\mu$M under the assumption of a simple

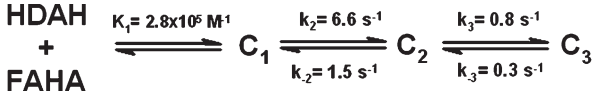


FIGURE 5: Postulated reaction mechanism of HDAH and FAHA.

reversible bimolecular binding model. This value is comparable with binding constants for binding of HDAH to other hydroxamates, e.g., SAHA (1.0 $\mu$M) and CypX (1.4 $\mu$M) (*18*). FAHA can be displaced from its complex with HDAH by hydroxamate inhibitors like SAHA. From the analysis of the monoexponential dissociation kinetics induced by the addition of excess SAHA to a preformed complex consisting of HDAH and FAHA, an apparent off rate of $0.15\ s^{-1}$ was determined. The rather simple one-exponential dissociation curve indicates a dominating unimolecular dissociation step. This observation is compatible with the single dissociation step in a simple reversible one-step equilibrium, but the possibility that the observed dissociation step is the rate-limiting step within a more complex overall reaction mechanism cannot be ruled out. To shed more light on the underlying mechanism, the association kinetics of HDAH and FAHA were investigated with a series of stopped-flow experiments at different FAHA concentrations. The binding reactions were performed under standard assay and pseudo-first-order conditions with respect to FAHA concentration. The association kinetics clearly showed a biexponential decay of tryptophan fluorescence at all FAHA concentrations (Figure 2). A closer look at the reciprocal time constants of both phases revealed that the reciprocal time constants of the fast phase approached

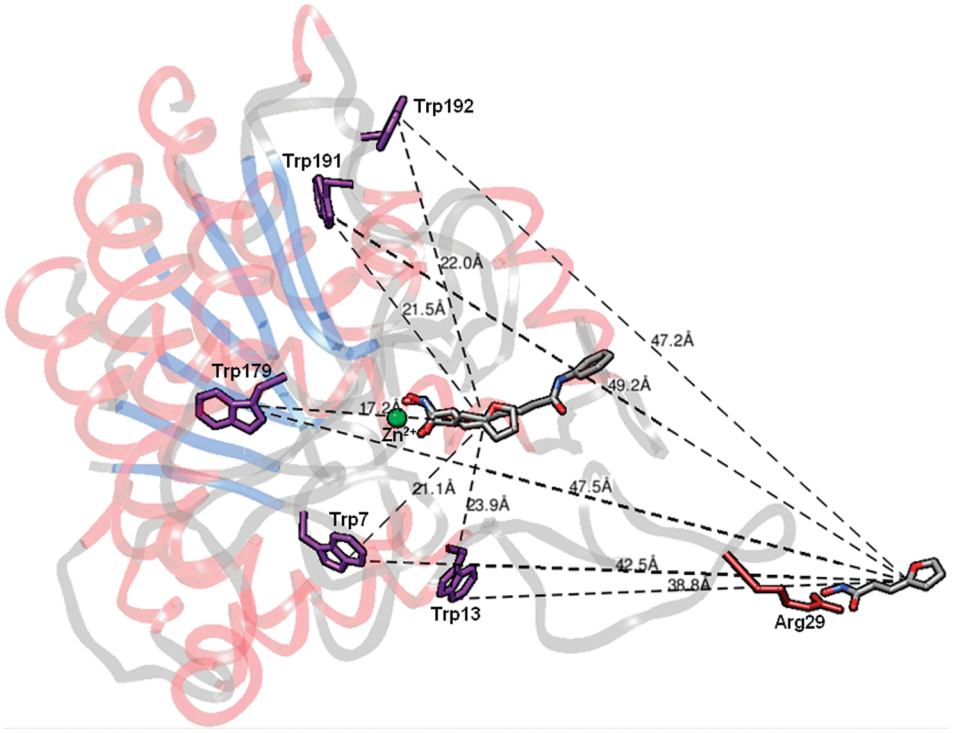


FIGURE 6: Overlay of the HDAH−SAHA structure (chain A of the tetramer) and FAHA. FAHA and SAHA are shown as stick models colored by element. HDAH is foreshadowed in the background for the most part. The five intrinsic tryptophan residues (violet), Arg29 (brown) at the outside, and $Zn^{2+}$ (green) at the bottom of the active site are accentuated. FAHA is shown twice, superimposed on SAHA in the active site of the HDAH−SAHA complex and attached to the Arg29 residue at the surface of the enzyme. The dotted straight lines connect the chromophores of the tryptophan residues and both FAHA molecules. The corresponding distances are given in angstroms.

a plateau at a concentration higher than ~8 $\mu$M FAHA (Figure 4A), whereas the reciprocal time constant of the slower phase exhibited a small increase below 2 $\mu$M but remained constant at higher concentrations of FAHA. Moreover, in the general case of a two-step system, where the two observed processes correspond to the two steps of the mechanism, both the sum and the product of the two reciprocal time constants are expected to give straight lines when plotted versus the concentration of FAHA (*21*). As one can see in panels C and D of Figure 4, both plots clearly deviate from linearity and rather show a curved dependence on FAHA concentration. This observation provides strong evidence for a complex reaction mechanism consisting of more than two steps or the existence of more than one type of HDAH conformer that is not readily interchangeable and shows different dynamics for interacting with FAHA. There are three lines of evidence that converge to a distinct likeliness for a homogeneous population of HDAH molecules. The first argument is based on the observed one-exponential dissociation curve of the HDAH−FAHA complex (Figure 3). If there would be two or more types of HDAH conformers, they may form different complexes with FAHA and dissociate at different rates. The second argument utilizes the reaction of HDAH with fluorescamine (unpublished results). In general, fluorescamine is used to create fluorescent conjugates of proteins, peptides, or amino acids containing a primary amino group. According to the reaction of alanine with fluorescamine (*24*), a series of kinetic experiments under pseudo-first-order conditions and a high excess of fluorescamine over HDAH revealed solely one-exponential reaction curves. Further analysis of the concentration dependence of the corresponding time constants was in agreement with a two-step mechanism involving one molecular species of HDAH. The ratio of the association and dissociation rates, $k_1/k_{-1}$, of the first reversible step was determined to be 0.9 $mM^{-1}$, and the rate constant for the irreversible second step, $k_2$, is 77.5 $s^{-1}$. These values were of the same order of magnitude as those estimated by Stein et al. (*24*) for the reaction of alanine with fluorescamine ($k_1/k_{-1}$ = 0.2 $mM^{-1}$, and $k_2$ = 100 $s^{-1}$). This means that HDAH behaves like a homogeneous population of molecules when reacting with fluorescamine. The third argument for the existence of one type of HDAH conformer is based on denaturation experiments with HDAH in the presence and absence of the inhibitor CypX (*25*). In that study, the denaturation of HDAH or HDAH−CypX complexes was initiated by mixing with concentrated solutions of guanidine hydrochloride in a stopped-flow instrument. All denaturation experiments at final denaturant concentrations of 2.4, 2.8, and 3.2 M showed distinct one-exponential curves which also militate against a mixture of HDAH conformers. While it is very difficult to directly prove the conformational homogeneity of HDAH, our line of arguments suggests that the existence of two or more types of HDAH conformers is rather unlikely.

The fact that both measurable time constants remain constant above 8 $\mu$M FAHA suggests that both corresponding phases represent unimolecular processes that are not directly dependent on FAHA. The equilibrium titration experiment shows that formation of the HDAH complex with FAHA is not complete at < 8 $\mu$M (Figure 1). With a combination of the equilibrium and kinetic results, it appears probable that there is a fast pre-equilibrium that limits the two observed consecutive unimolecular processes. This raises the question of why this first association step does not generate a measurable FRET signal, though FAHA and HDAH must form an intermediate complex, $C_1$ (Figure 5), where HDAH and FAHA come into close contact.

In principle, the pre-equilibrium could be nonaccessible, because of an extremely fast establishment during mixing within

the stopped-flow instrument before the data are recorded. The dead time of the instrument under the conditions of the experiment was determined to be ~2 ms. A thorough investigation of the very fast time range of the fluorescence signal of alternating mixtures of HDAH with FAHA and assay buffer proved that there was no measurable very fast FRET signal. An alternative explanation for the missing FRET signal of the postulated fast pre-equilibrium could be that the distance between FAHA and HDAH in the first complex, $C_1$, would be too long to generate a measurable FRET signal. To test this hypothesis, we superimposed the lowest-energy conformer of FAHA (estimated using MarvinSketch from ChemAxon version 5.1.5) on SAHA within the active site of the determined crystal structures of the HDAH−SAHA complex (*13*) by minimizing the root-mean-square distance between the heavy atoms of the corresponding hydroxamate groups and pairs of the four adjacent carbon atoms (Figure 6).

The average distance between the donor tryptophan residues and FAHA positioned within the active site was estimated to be ~21 Å. If we assume that FAHA binds to the outer surface of HDAH in the first association step, it may interact with, e.g., the positively charged Arg29 in the outer loop (Asp15−Leu37) close to the entrance of the active site channel. The averaged distance between the outside bound FAHA and the tryptophan residues would be ~45 Å. For this hypothetical distance, the theoretical energy transfer efficiency can be calculated according to eq 7 to be as low as 0.01. Such a small effect on the donor fluorescence would certainly be overlooked under the conditions of the stopped-flow experiment. Hence, FAHA may bind to the surface of HDAH at first without generating a measurable FRET before it moves into the active site. The two slower unimolecular processes, which can be measured, are interpreted as conformational changes in FAHA−HDAH complexes $C_1$ and $C_2$ (Figure 5).

The kinetic and spectroscopic data prove that there is no direct binding of FAHA to the interior of the active site. The access to the active site must be hindered, probably due to an unfavorable initial conformation of HDAH. A conformational change in the initial complex, $C_1$, may open the way to the active site and be reflected by the first observed relatively slow phase. Once there is free access to the active site, the outside bound inhibitor can translocate rapidly into the interior of the enzyme, generating a pronounced FRET signal in complex $C_2$. The third step could be an additional inhibitor-induced conformational rearrangement of $C_2$, which stabilizes the final complex, $C_3$. All kinetic data for the binding reaction were analyzed according to eqs 4 and 5, yielding the association constant of the fast equilibrium ($K_1$ = $0.28 \times 10^6$ $M^{-1}$) and the rate constants of the consecutive conformational changes ($k_2$ = 6.6 $s^{-1}$, $k_{-2}$ = 1.5 $s^{-1}$, $k_3$ = 0.8 $s^{-1}$, and $k_{-3}$ = 0.3 $s^{-1}$). The apparent dissociation rate constant of 0.15 $s^{-1}$, which has been determined in a displacement experiment, reflects the rate-limiting step in the dissociation of the FAHA−HDAH complex. The apparent dissociation constant is assigned to the rate-limiting dissociation of the final complex, $C_3$, because the corresponding time constants are similar.

The mechanism by which inhibitors interact with enzymes has been investigated by many researchers. Many enzymes are reported to be inhibited in a one-step mechanism (*26*−*28*). Some other studies report two-step reactions, in which a rapid pre-equilibrium is followed by a slower conformational change leading to a more stable complex (*29*−*31*). However, there are only a few studies, e.g., with cytochrome P4503A4 (*32*) and thrombin (*33*), that have found an enzyme inhibition mechanism consisting of three or more steps like in our study. It is not unexpected that different enzymes exhibit different modes of inhibition. These mechanistic differences are not obvious from crystal or NMR enzyme−inhibitor complexes. Our study proves once more that structural and kinetic data complement each other and improve our understanding of the molecular processes. Further studies with different inhibitors from the same or other structural classes that must generate a specific measurement signal could be used to learn more about the influence of inhibitor structure not only on the speed but also on the mechanism of interaction with HDAH.

In conclusion, all kinetic data of this study are in agreement with a reversible three-step mechanism for the inhibition of HDAH by FAHA. Kinetic and spectroscopic data suggest a fast pre-equilibrium, where FAHA binds to the surface of HDAH. A subsequent conformational change of the first complex is supposed to open access to the interior of the enzyme accompanied by a rapid translocation of the inhibitor into the active site. The last step is considered as a conformational rearrangement to further stabilize the final complex. The location of the postulated preliminary binding site at the surface of HDAH and the consideration of the observed distinct conformational changes of intermediate HDAH−FAHA complexes may provide some new clues for the development of novel lead structures.

## REFERENCES


1. Mai, A., Massa, S., Rotili, D., Cerbara, I., Valente, S., Pezzi, R., Simeoni, S., and Ragno, R. (2005) Histone deacetylation in epigenetics: An attractive target for anticancer therapy. *Med. Res. Rev. 25*, 261–309.
2. Lehrmann, H., Pritchard, L. L., and Harel-Bellan, A. (2002) Histone acetyltransferases and deacetylases in the control of cell proliferation and differentiation. *Adv. Cancer Res. 86*, 41–65.
3. Grunstein, M. (1997) Histone acetylation in chromatin structure and transcription. *Nature 389*, 349–352.
4. Peterson, C. L. (2002) HDAC's at work: Everyone doing their part. *Mol. Cell 9*, 921–922.
5. Mariadason, J. M., Corner, G. A., and Augenlicht, L. H. (2000) Genetic reprogramming in pathways of colonic cell maturation induced by short chain fatty acids: Comparison with trichostatin A, sulindac, and curcumin and implications for chemoprevention of colon cancer. *Cancer Res. 60*, 4561–4572.
6. Peart, M. J., Smyth, G. K., van Laar, R. K., Bowtell, D. D., Richon, V. M., Marks, P. A., Holloway, A. J., and Johnstone, R. W. (2005) Identification and functional significance of genes regulated by structurally different histone deacetylase inhibitors. *Proc. Natl. Acad. Sci. U.S.A. 102*, 3697–3702.
7. Xu, W. S., Parmigiani, R. B., and Marks, P. A. (2007) Histone deacetylase inhibitors: Molecular mechanisms of action. *Oncogene 26*, 5541–5552.
8. Marks, P. A., and Dokmanovic, M. (2005) Histone deacetylase inhibitors: Discovery and development as anticancer agents. *Expert Opin. Invest. Drugs 14*, 1497–1511.
9. Minucci, S., and Pelicci, P. G. (2006) Histone deacetylase inhibitors and the promise of epigenetic (and more) treatments for cancer. *Nat. Rev. Cancer 6*, 38–51.
10. Paris, M., Porcelloni, M., Binaschi, M., and Fattori, D. (2008) Histone deacetylase inhibitors: From bench to clinic. *J. Med. Chem. 51*, 1505–1529.
11. Riester, D., Hildmann, C., and Schwienhorst, A. (2007) Histone deacetylase inhibitors: Turning epigenic mechanisms of gene regulation into tools of therapeutic intervention in malignant and other diseases. *Appl. Microbiol. Biotechnol. 75*, 499–514.
12. Lee, M. J., Kim, Y. S., Kummar, S., Giaccone, G., and Trepel, J. B. (2008) Histone deacetylase inhibitors in cancer therapy. *Curr. Opin. Oncol. 20*, 639–649.
13. Nielsen, T. K., Hildmann, C., Dickmanns, A., Schwienhorst, A., and Ficner, R. (2005) Crystal structure of a bacterial class 2 histone deacetylase homologue. *J. Mol. Biol. 354*, 107–120.

14. Hildmann, C., Ninkovic, M., Dietrich, R., Wegener, D., Riester, D., Zimmermann, T., Birch, O. M., Bernegger, C., Loidl, P., and Schwienhorst, A. (2004) A new amidohydrolase from *Bordetella* or *Alcaligenes* strain FB188 with similarities to histone deacetylases. *J. Bacteriol. 186*, 2328–2339.
15. Hildmann, C., Wegener, D., Riester, D., Hempel, R., Schober, A., Merana, J., Giurato, L., Guccione, S., Nielsen, T. K., Ficner, R., and Schwienhorst, A. (2006) Substrate and inhibitor specificity of class 1 and class 2 histone deacetylases. *J. Biotechnol. 124*, 258–270.
16. Riester, D., Hildmann, C., Haus, P., Galetovic, A., Schober, A., Schwienhorst, A., and Meyer-Almes, F. J. (2009) Non-isotopic dual parameter competition assay suitable for high-throughput screening of histone deacetylases. *Bioorg. Med. Chem. Lett. 19*, 3651–3656.
17. Schafer, S., Saunders, L., Eliseeva, E., Velena, A., Jung, M., Schwienhorst, A., Strasser, A., Dickmanns, A., Ficner, R., Schlimme, S., Sippl, W., Verdin, E., and Jung, M. (2008) Phenylalanine-containing hydroxamic acids as selective inhibitors of class IIb histone deacetylases (HDACs). *Bioorg. Med. Chem. 16*, 2011–2033.
18. Riester, D., Hildmann, C., Schwienhorst, A., and Meyer-Almes, F. J. (2007) Histone deacetylase inhibitor assay based on fluorescence resonance energy transfer. *Anal. Biochem. 362*, 136–141.
19. Bouchain, G., and Delorme, D. (2003) Novel hydroxamate and anilide derivatives as potent histone deacetylase inhibitors: Synthesis and antiproliferative evaluation. *Curr. Med. Chem. 10*, 2359–2372.
20. Munster, P. N., Troso-Sandoval, T., Rosen, N., Rifkind, R., Marks, P. A., and Richon, V. M. (2001) The histone deacetylase inhibitor suberoylanilide hydroxamic acid induces differentiation of human breast cancer cells. *Cancer Res. 61*, 8492–8497.
21. Bernasconi, C. (1976) Relaxation Kinetics Academic Press, Inc., New York.
22. Lasdon, L. S., Waren, A. D., Jain, A., and Ratner, M. (1978) Design and Testing of a Generalized Reduced Gradient Code for Nonlinear Programming, 4th ed., pp 34−50, Association for Computing Machinery, New York.
23. Foerster, T. (1948) Zwischenmolekulare Energiewanderung und Fluoreszenz, 2nd ed.; Annalen der Physik, 1948, Vol. 437, pp 55−75.
24. Stein, S., Bohlen, P., and Udenfriend, S. (1974) Studies on the kinetics of reaction and hydrolysis of fluorescamine. *Arch. Biochem. Biophys. 163*, 400–403.
25. Kern, S., Riester, D., Hildmann, C., Schwienhorst, A., and Meyer-Almes, F. J. (2007) Inhibitor-mediated stabilization of the conformational structure of a histone deacetylase-like amidohydrolase. *FEBS J. 274*, 3578–3588.
26. Navarro-Martinez, M. D., Cabezas-Herrera, J., Garcia-Canovas, F., and Rodriguez-Lopez, J. N. (2007) Inhibition of *Stenotrophomonas maltophilia* dihydrofolate reductase by methotrexate: A single slow-binding process. *J. Enzyme Inhib. Med. Chem. 22*, 377–382.
27. Wielgus-Kutrowska, B., Antosiewicz, J. M., Dlugosz, M., Holy, A., and Bzowska, A. (2007) Towards the mechanism of trimeric purine nucleoside phosphorylases: Stopped-flow studies of binding of multi-substrate analogue inhibitor -2-amino-9-[2-(phosphonomethoxy)ethyl]-6-sulfanylpurine. *Biophys. Chem. 125*, 260–268.
28. Ploux, O., Breyne, O., Carillon, S., and Marquet, A. (1999) Slow-binding and competitive inhibition of 8-amino-7-oxopelargonate synthase, a pyridoxal-5′-phosphate-dependent enzyme involved in biotin biosynthesis, by substrate and intermediate analogs. Kinetic and binding studies. *Eur. J. Biochem. 259*, 63–70.
29. Faller, B., Cadene, M., and Bieth, J. G. (1993) Demonstration of a two-step reaction mechanism for the inhibition of heparin-bound neutrophil elastase by $\alpha_1$-proteinase inhibitor. *Biochemistry 32*, 9230–9235.
30. Furfine, E. S., D'Souza, E., Ingold, K. J., Leban, J. J., Spector, T., and Porter, D. J. (1992) Two-step binding mechanism for HIV protease inhibitors. *Biochemistry 31*, 7886–7891.
31. Rajagopalan, R., Misialek, S., Stevens, S., Myszka, D., Brandhuber, B., Ballard, J., Andrews, S., Seiwert, S., and Kossen, K. (2009) Inhibition and Binding Kinetics of the Hepatitis C Virus NS3 Protease Inhibitor ITMN-191 Reveals Tight Binding and Slow Dissociative Behavior. *Biochemistry. 48*, 2559–2568.
32. Isin, E. M., and Guengerich, F. P. (2007) Multiple sequential steps involved in the binding of inhibitors to cytochrome P450 3A4. *J. Biol. Chem. 282*, 6863–6874.
33. Jackman, M. P., Parry, M. A., Hofsteenge, J., and Stone, S. R. (1992) Intrinsic fluorescence changes and rapid kinetics of the reaction of thrombin with hirudin. *J. Biol. Chem. 267*, 15375–15383.